

Effect of Mn²⁺ Doping on Structural, Morphological and Optical Properties of ZnS Nanoparticles by Chemical Co-Precipitation Method

L. Sujata Devi^{a*}, K. Nomita Devi^b, B. Indrajit Sharma^a, H. Nandakumar Sarma^b

^aDepartment of Physics, Assam University, Silchar-788011, Assam, India

^bDepartment of Physics, Manipur University, Canchipur, Imphal-795003, India

Abstract: Zinc Sulphide (ZnS) nanoparticles doped with different concentrations of Mn²⁺ (0%, 2%, 4%, 6%, 8%, 10%) have been synthesized by chemical co-precipitation method using polyvinyl alcohol (PVA) as a capping agent to control the particle growth. The structural characterizations of as synthesized nanoparticles are determined by X-ray diffraction (XRD) which showed cubic zinc blende structures with average crystallite sizes of the range 2.3 nm - 2.1 nm. There is no phase transformation due to Mn²⁺ doping and this characteristic has been observed in all the synthesized powder. Scanning electron microscopy (SEM) and energy dispersive X-ray (EDX) analysis show the morphology and elemental analysis of as synthesized nanoparticles. TEM images confirms the spherical shape of the nanoparticles. HRTEM and SAED images show the crystalline nature and confirm the cubic nature of ZnS nanoparticles. Absorption study has been carried out by using UV-Vis spectrophotometer to determine the band gap of ZnS:Mn nanoparticles and they showed a blue shift with respect to the bulk. The effect of Mn²⁺ substitution on the photoluminescence properties of doped samples is also studied and doped ZnS:Mn showed enhanced luminescence property compared with that of the undoped ZnS nanoparticles. Radius of the synthesized nanoparticles has been evaluated from the absorption spectrum by using the Effective Mass Approximation (EMA) formula. Fourier Transform Infrared Spectra (FTIR) is recorded in an FTIR spectrometer to verify the presence and effect of capping agent.

Keywords: XRD, PVA, chemical co-precipitation, UV-Vis Spectrophotometer, photoluminescence, FTIR

I. Introduction:

Researchers take keen interest in the semiconductor of Group II-VI compounds because of their important unique properties and potential applications [1-5]. ZnS is an important group II-VI semiconductor material with a wide band gap of 3.54 eV at room temperature [6]. Not only did it has attracted a lot of research due to its excellent properties at nanoscale and low toxicity when compared to other chalcogenides [7-10], it has been also been extensively investigated due to its potential for device applications like optical coatings, field effect transistor, optical sensors, electroluminescence displays, phosphors and other light emitting materials [11, 12]. Because of its wide band gap, it has a high index of reflection and high transmittance in the visible range particularly suitable for host material for a large variety of dopants. The synthesis of Mn²⁺ doped ZnS nanoparticles have been mainly studied due to luminescence of manganese ions inside the ZnS host. In Mn²⁺ doped ZnS nanoparticles, the luminescence quantum efficiency is expected to increase as a result of greater interaction between the electron and hole of the host ZnS nanoparticles with localized dopant levels [13]. In photoluminescence, the electrons are excited from the ZnS valence band to conduction band by absorbing the energy equal to or greater than their band gap energy subsequent relaxation of these photo-excited electrons to some surface states or levels is followed by radiative decay enabling luminescence in the visible region.

It is well known that semiconductor nanoparticles are themselves highly unstable and in the absence of the capping agent, they agglomerate very rapidly [14]. For this reason, bonding of capping agent to nanoparticles is necessary to provide chemical passivation and also to improve the surface state which has substantial influence on the optical and electronic properties of nanoparticles [15]. As the surface of the nanoparticle is very high, agglomeration takes place which result in the increase of the size of the particle. So in order to control the agglomeration, we have used polyvinyl alcohol as a capping agent especially during synthesis. In addition, the viscosity of the polymer solution will be helpful in controlling the growth of the nanoparticles and thus prevent particles from aggregating and hence no stabilizers will be needed.

There are several methods to synthesize PVA capped ZnS nanoparticles with various Mn²⁺ concentration such as sol-gel, chemical vapour deposition, chemical co-precipitation method and hydrothermal method [16-19]. So among the different synthesis processes, chemical co-precipitation method is used because of its manifold advantages like simple, easy handling, economical and capability for large scale production. Till now, there are many reports on the synthesis and characterization of PVA capped ZnS nanoparticles doped with various concentration of Mn²⁺. But, it still require further investigation so as to study more on the structural,

optical and electrical properties with due emphasis given on the luminescence property for its use as a suitable candidate for various device applications.

II. Experimental Details:

The chemicals used in this work are zinc acetate [Zn(CH₃COO)₂·2H₂O], sodium sulphide flakes [Na₂S], manganese acetate tetrahydrate [Mn(CH₃COO)₂·4H₂O], 2 grams of PVA which acts as a capping agent to control the agglomeration of particles size and deionised water as dispersing solvent.

ZnS nanoparticles doped with different concentrations of Mn²⁺ were synthesized by chemical co-precipitation method. 6.585 gm of zinc acetate [Zn(CH₃COO)₂·2H₂O] was dissolved in deionised water and stirred for 15 minutes at room temperature to achieve complete dissolution. Manganese acetate tetrahydrate [Mn(CH₃COO)₂·4H₂O] of varying concentration and sodium sulphide [Na₂S] was also dissolved in deionised water and stirred separately. Then 2 gram of PVA was added to the reaction medium to control the particle size and stirred for 1 hour. Afterwards Na₂S solution was added drop by drop to the prepared solution which was maintained at a pH value of 6 and stirred continuously for 2 hours at room temperature. In the final step, the white precipitate obtained was filtered using Whatman 40 filter paper. To remove the last traces of adhered impurities, the precipitate was washed several times using deionised water and dried at 60°C for 24 hours. After sufficient drying, the precipitate was grinded in an agate mortar to achieve fine powder for further analysis.

The structure and phase of the as synthesized samples were determined by X-ray diffraction (XRD) using P-Analytical X-ray diffractometer using Cu-K_α (λ=1.540 Å) radiation. Diffraction patterns had been recorded over the 2θ range of 20° to 80° at the scan rate of 2° per minute.

The shape and particle size were studied using JEOL JEM 2010 Transmission electron microscope (TEM) operated at 200 kV accelerating voltage. The lattice fringes and diffraction pattern of the as synthesized samples were determined by HRTEM and SAED. The surface morphology and elemental analysis of the synthesized samples were studied by FEI Quanta 250 Scanning electron microscope (SEM) and Energy dispersive X-ray (EDX) spectrum (Quanta 250). The optical absorbance spectra for the synthesized samples were recorded using UV-vis spectrophotometer (Perkin-Elmer Lambda 35) in the wavelength range of 350 nm - 700 nm. The measurements are done in the wavelength scanning mode at room temperature in the normal incidence and using uncoated glass slides as the reference. The room temperature photoluminescence spectra of the synthesized sample were measured to study the luminescence properties of the nanoparticles using Perkin Elmer LS 55 with an excited light wavelength of 340 nm. FTIR were recorded using SHIMADSU 8400S spectrophotometer to verify the presence and effect of the capping agent.

III. Result And Discussions:

3.1. Structural analysis:

The crystalline structure of the synthesized samples were recorded with the X-ray diffraction using Cu-K_α radiation (λ=1.540 Å). The intensity data were collected over a 2θ range of 20° - 80°. The XRD pattern of as synthesized samples are shown in figure 1. The patterns indicate that all the samples are consistent with cubic zinc blende structure of ZnS which are in close agreement with the standard ICDD (International Center for Diffraction Data) card number 80-0020. From the XRD patterns, the broadening of the diffraction peaks of the nanoparticles is obvious which reflects the characteristic of nano sized materials. The most prominent peak observed in the figure corresponds to the lattice plane of (1 1 1). Two other peaks corresponding to the lattice plane (2 2 0) and (3 1 1) are observed with varying intensities. There is no phase transformation due to Mn²⁺ doping to ZnS host. The peaks in the diffraction pattern of Mn²⁺ doped ZnS shows a clear shift towards higher 2θ values with increasing Mn²⁺ concentration. The increase in diffraction angle is clearly a result of lattice contraction expected to occur because of higher surface to volume ration [20]. This shift may also be due to occupation of Mn²⁺ ions at Zn sites.

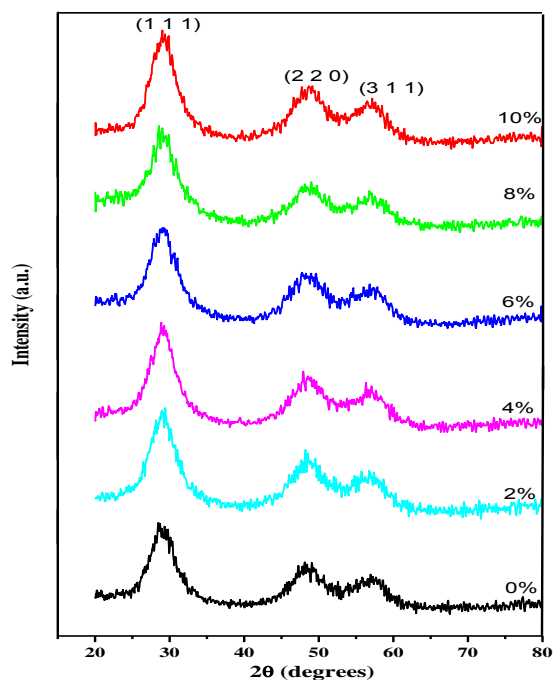


Figure 1: XRD pattern of ZnS nanoparticles doped with different concentrations of Mn^{2+}

The synthesized ZnS nanoparticles doped with different concentration of Mn^{2+} are found to be mainly cubic phase, the lattice parameter $a=b=c$ was calculated using equation [21]

$$a = d\sqrt{h^2 + k^2 + l^2} \quad (1)$$

The corrected value of lattice constant is estimated from the intercept of the Nelson-Riley plots which is a graph of the calculated values of lattice constant for different planes versus error function give by

$$f(\theta) = \frac{1}{2} \left(\frac{\cos^2 \theta}{\sin \theta} + \frac{\cos^2 \theta}{\theta} \right) \quad (2)$$

The intercept of this plot with x-axis gives the corrected value of lattice constant. Therefore, the values obtained from N-R plots are more or less free from systematic error.

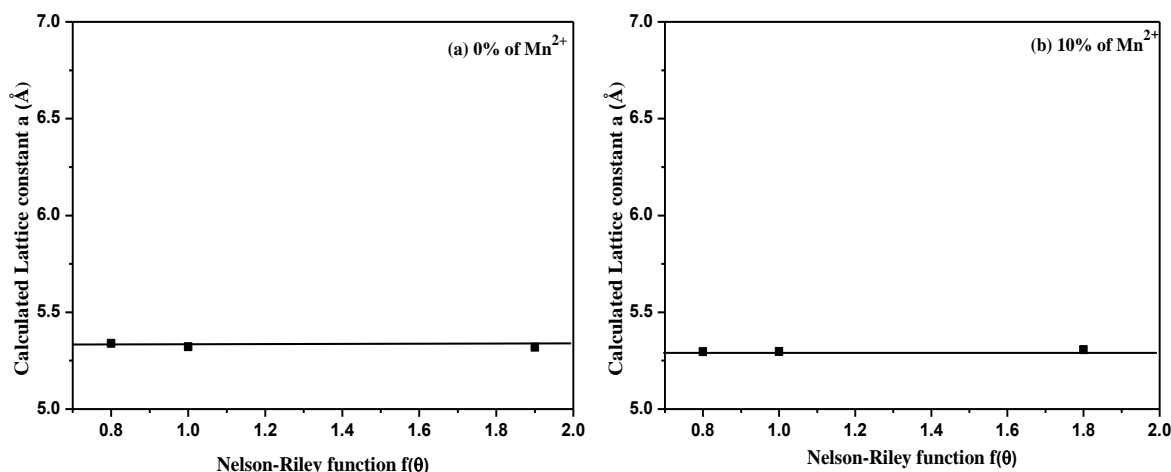


Figure 2: Nelson Riley Plot for ZnS nanoparticles doped with 0% and 10% of Mn^{2+}

The average crystallite size of ZnS nanoparticles doped with different concentration of Mn^{2+} were calculated from the Full width at half maximum (FWHM) of the most prominent diffraction peak by using the Debye-Scherrer formula [22]

$$D = \frac{k\lambda}{\beta \cos \theta} \quad (3)$$

where D is the average crystallite size, k is the proportionality constant with a value taken to be 0.94, λ is the wavelength of the Cu-K α used ($\lambda=1.540 \text{ \AA}$), θ is the angle of diffraction and β is the full width at half maximum in radians of XRD peaks. Hence by using the above relation, the evaluated crystallite size of PVA capped ZnS nanoparticles doped with different concentration of Mn²⁺ is in the range of 2.3 nm - 2.1 nm.

A dislocation is an imperfection in a crystal associated with the misregistry of the lattice in one part of the crystal with that in another part. Unlike vacancies and interstitial atoms, dislocations are not equilibrium imperfections i.e. thermodynamic considerations are insufficient to account for their existence in the observed densities. In fact, the growth mechanism involving dislocation is a matter of importance. Thus the dislocation density (δ) is defined as the length of dislocation lines per unit volume of the crystal and was evaluated by using the relation [23]

$$\delta = \frac{n}{D^2} \quad (4)$$

where ‘ D ’ is the crystallite size obtained from XRD data and ‘ n ’ is a factor which is equal to unity giving minimum dislocation density.

The origin of strain is related to lattice ‘mis-fit’ which in turn depends upon the growth condition. The microstrain ϵ_{hkl} developed in the synthesized sample was calculated by using the relation [24].

$$\epsilon_{hkl} = \frac{\beta \cos \theta}{4} \quad (5)$$

Using this relation, magnitude of lattice strain (ϵ_{hkl}) along the most preferred orientation is calculated for PVA capped ZnS nanoparticles doped with different concentration of Mn²⁺. Table 1 shows crystallite size, lattice parameter, strain and dislocation densities of ZnS nanoparticles doped with different concentrations of Mn²⁺. From the table we have seen that as the crystallite decreases, lattice strain and dislocation density slightly increases.

Table 1: Crystallite size, lattice parameter, strain and dislocation density of ZnS nanoparticles doped with different concentrations of Mn²⁺

Doping concentration (%)	Crystallite size (nm)	$a=b=c$ from N-R plot (\AA)	Strain $\times 10^{-3}$	Dislocation density $\times 10^{16} (m^{-2})$
0	2.3	5.339	15.68	18.90
2	2.2	5.334	16.11	20.66
4	2.2	5.313	16.48	20.66
6	2.1	5.306	16.83	22.67
8	2.4	5.301	15.30	17.36
10	2.2	5.288	16.40	20.66

The shape and particle size of the synthesized samples were investigated through Transmission electron microscope (TEM). Figure 3(a) shows the TEM image of undoped ZnS which reveals that particles are nearly spherical shaped having sizes in the range of 3.45 nm – 5.47 nm and is found to be larger than that obtained from XRD because XRD assumed regular atomic arrangement in the synthesized samples whereas TEM gives full size of the particles including non-crystalline part also [25]. Figure 3(b) shows the corresponding HRTEM image which shows clearly the formation of lattice fringes, indicating the crystalline nature of the as synthesized samples. There are also discontinuities in the lattice fringes which are due to the dislocation and stacking faults which further confirm oriented attachment growth among the nanoparticles. Figure 3(c) shows the corresponding selected area electron diffraction (SAED) pattern of the as synthesized samples. The diffraction pattern consists of a central hole with concentric broad rings around it. The rings corresponds to reflections from the (1 1 1), (2 2 0) and (3 1 1) planes confirming the cubic structure of ZnS nanoparticles.

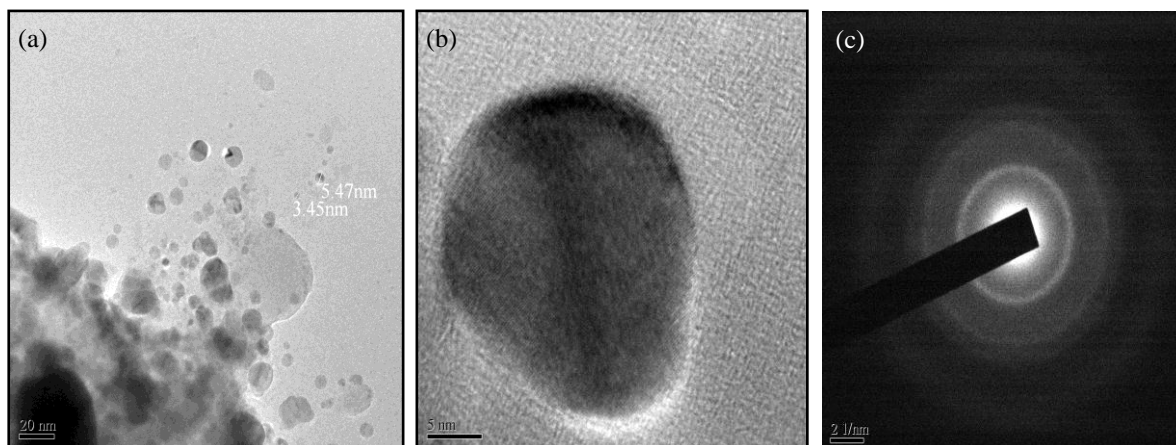


Figure 3(a-c): TEM, HRTEM and SAED pattern of undoped ZnS nanoparticles.

3.2. Morphology and elemental analysis:

Figure 4(a-b) shows the SEM micrographs of the synthesized samples. The micrographs show that the particles had a rough morphology and spongy surface as a result of the passivation by PVA. Due to these reasons, it is difficult to determine the particle size of the synthesized samples.

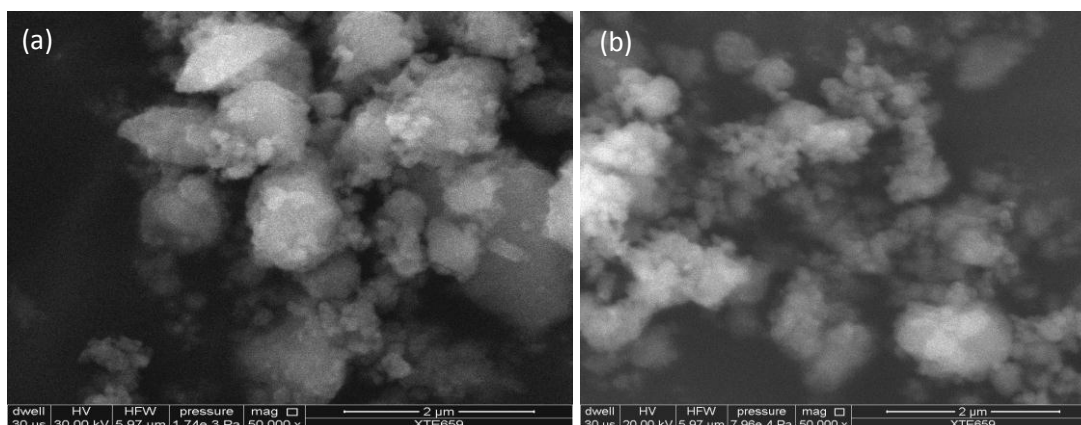


Figure 4: SEM images of ZnS nanoparticles with (a) 0% and (b) 10% of Mn^{2+}

Figure 5(a & b) shows the EDX spectra for 0% and 10% which revealed the presence of strong peaks for Zn and S and a detectable amount of Mn^{2+} which is due to low doping concentration of Mn^{2+} . But in the figure, small peak oxygen is present. This oxygen may be incorporated into the synthesized nanoparticles either from the atmosphere or from the aqueous medium of the solution resulting in higher amount of oxygen contamination [26].

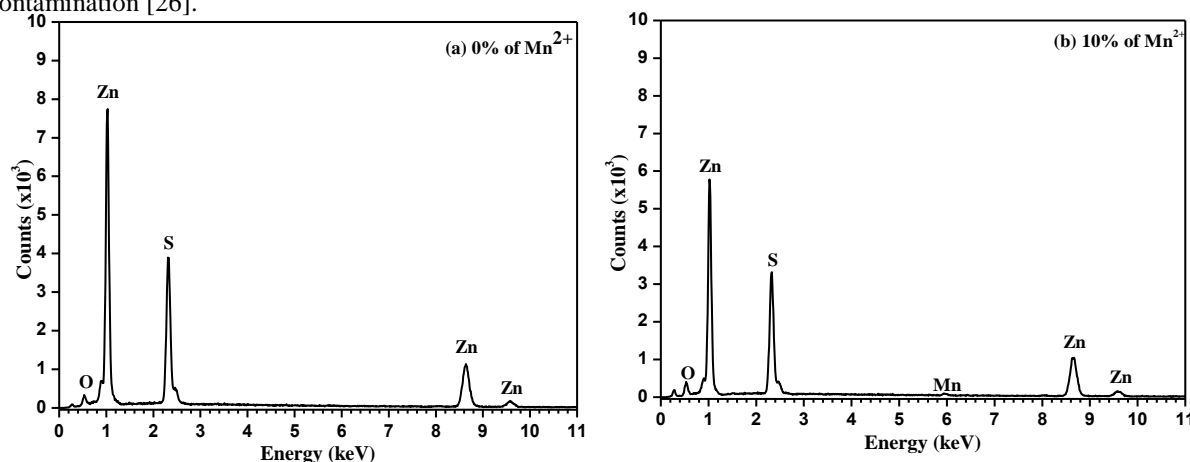


Figure 5: EDX spectra for (a) 0% and (b) 10% of Mn^{2+} doped ZnS nanoparticles

IV. Optical Results:

4.1. UV-vis (Ultra Violet-visible) Spectroscopy:

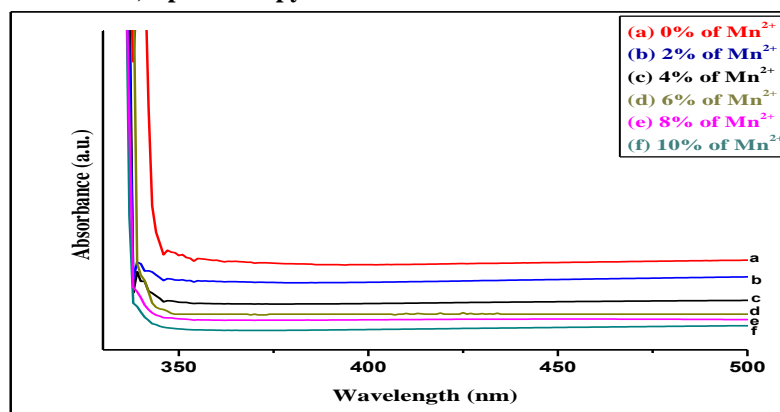


Figure 6: UV-vis absorption spectra of ZnS nanoparticles doped with varying concentration of Mn²⁺

The optical absorption spectra of Zn_{1-x}Mn_xS (where x is equal to 0%, 2%, 4%, 6%, 8% and 10%) samples at room temperature by a UV-vis spectrophotometer in the range 300 nm-500 nm are shown in figure 6. From the absorption spectra, it is seen that the absorption edge of ZnS nanoparticles is fairly blue shifted when compared with that of bulk ZnS (3.54 eV ≈ 348 nm). ZnS has good absorption for light in the wavelength of 220 nm - 350 nm [27]. However, the absorption edge of the doped samples is shifted towards shorter wavelength when compared with undoped ZnS and this shift slightly decreases with increase in Mn²⁺ concentration. This blue shift is mainly attributed to a strong quantum confinement effect caused by the reduction in particle size [28]. The shift towards shorter wavelength indicates an increase in the optical band gap.

It is well known that the fundamental absorption is due to the transition of electron excitation from the valence band to the conduction band which can be used to determine the value of the optical band gap of the nanoparticles. The most direct way of extracting the optical band gap from the figure is to simply determine the wavelength at which the extrapolation of the base line and the absorption edge crossed [29]. Thus the corresponding absorption edges for 0%, 2%, 4%, 6%, 8% and 10% of ZnS:Mn are 347 nm, 345 nm, 345 nm, 344 nm, 342 nm and 343 nm respectively. The energy band gaps of all the prepared samples were calculated by using a simple wave-energy equation

$$E_g^{nano} = h\nu_g^{nano} = \frac{hc}{\lambda_g^{nano}} \quad (6)$$

where h is the Planck's constant, c is the velocity of light, λ is the absorption wavelength and E_g^{nano} is the energy band gap of the semiconductor nanoparticle in the absorption spectra. Through calculation, the optical energy band gap for ZnS nanoparticles doped with 0, 2, 4, 6, 8 and 10% concentrations of Mn²⁺ are 3.55, 3.57, 3.57, 3.58, 3.60 and 3.59 eV respectively and these are larger than the band gap of bulk ZnS (3.54 eV) due to quantum confinement effect.

Effective mass approximation (EMA) as proposed [30, 31] has been used to explain the theory of blue shift and energy gap as a function of particle size. According to EMA, the equation derived for radius of particle is given by

$$\Delta E_g = E_g^{nano} - E_g^{bulk} = \frac{h^2}{8r^2} \left(\frac{1}{m_e^*} + \frac{1}{m_h^*} \right) - \frac{1.8e^2}{4\pi\epsilon_0 r} \quad (7)$$

where E_g^{nano} is the band gap energy of the nanoparticle as determined from the UV-vis absorbance spectrum, E_g^{bulk} is the band gap of the bulk ZnS at room temperature, r is the radius of the nanoparticles, $m_e^*=0.34 m_0$ and $m_h^*=0.23 m_0$, e is the electronic charge, h is the planck's constant, ϵ_0 is the vacuum permittivity and ϵ is the high frequency dielectric constant of ZnS and its value= 8.76.

The radii of the synthesized nanoparticles calculated for different concentrations from the above equation nearly match the crystallite size that is estimated from XRD. The value of the particle size estimated from EMA and XRD with different concentrations of Mn²⁺ are shown in table 2.

Table 2: Comparison of particle size estimated by EMA formula and XRD

Mn doping concentration (%)	Particle size from EMA (nm)	Crystallite size from XRD (nm)
0	3.2	2.3
2	3.0	2.2
4	3.0	2.2
6	2.8	2.1
8	2.6	2.4
10	2.8	2.2

4.2. Photoluminescence (PL):

The room temperature photoluminescence emission spectra of doped and undoped ZnS nanoparticles under excitation wavelength of 340 nm (4.37 eV) are shown in Figure 7.

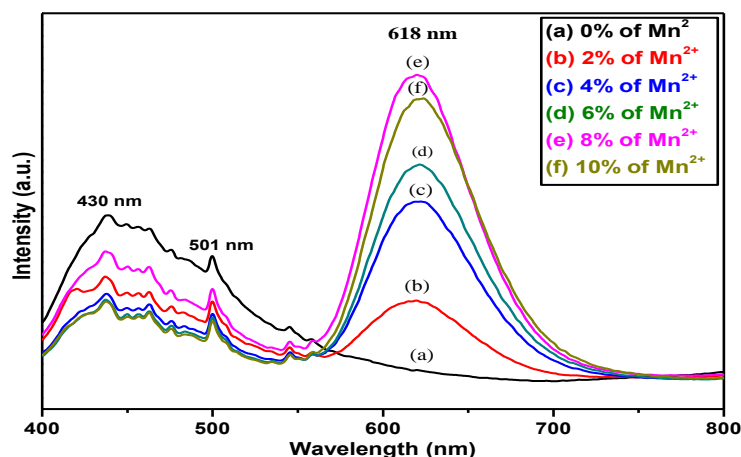


Figure 7: Emission spectra of ZnS nanoparticles doped with different concentrations of Mn^{2+}

From the figure, luminescence peaks at 430 nm (2.87 eV) and 501 nm (2.46 eV) are observed for all the samples in the emission spectra irrespective of the doping. The blue emission PL peak at about 430 nm is attributed due to the transition of electrons from the shallow states near the conduction band to sulphur vacancy present near the valence band. The other green emission PL peak at 501 nm is assigned to elemental sulphur species on the surface of ZnS nanoparticles. Also, from the figure we can see that the peak position of blue and green emission does not change with the increase in Mn^{2+} concentration which indicates that the energy level of sulphur vacancy relative to the valence band is nearly constant. In addition, some new weak emission peaks are observed which may be due to the excess of acetate in the prepared solution. But when Mn^{2+} ions are incorporated into the ZnS lattice and substituted the host cations sites, the s-p electrons of the host ZnS is mixed with the d-electrons of Mn^{2+} which makes the forbidden transition between excited (4T_1) and ground (6A_1) levels within the $3d^5$ orbital of Mn^{2+} . Generally, emission occurs through energy transfer from the excited state of ZnS host lattice to the d electrons of Mn^{2+} [32, 20]. This clearly suggests that the emission at 618 nm arises from Mn^{2+} ions of MnS nanoparticles. It is important to note that the Mn^{2+} ions in MnS nanoparticles have two emission peaks at 1.66 eV and 1.8 eV. Therefore, the presence of Mn^{2+} emission at 618 nm (1.99 eV) indicates that the Mn^{2+} ions occupy the Zn^{2+} host lattice. From the figure, concentration quenching is also observed when Mn^{2+} concentration is increased more than 8% where there is a decrease in the intensity of Mn^{2+} for ${}^4T_1 - {}^6A_1$ transition. Similar quenching effect on Mn^{2+} doped ZnS nanoparticles have also been reported by earlier workers [33-36]. It is worth mentioning that concentration quenching has been mainly attributed to the migration of the excitation energy between Mn^{2+} ions pairs in the case of Mn^{2+} doping. Thus the existence of Mn^{2+} pairs is important for the occurrence of the concentration effect. During the concentration process, the excitation energy is transferred from one Mn^{2+} ion to its nearest Mn^{2+} ion by non-radiative transitions and a via a number of transfer steps, finally to a quenching site (eg. defect state) [37]. From the figure, the relative intensity corresponding to blue and green peaks are suppressed as concentration of Mn^{2+} increases and reaches maximum at 8%. The decrease of the luminescent intensity at Mn^{2+} concentration of 10% may also be caused by the formation of MnS, though the XRD measurement did not show the existence of Mn phase. But it is evident that the ZnS:Mn powder colour is changed from white to light pink when the doping concentration is 10%. MnS particles not only act as non-radiative recombination centres but also reduced the number of Mn^{2+} ions that are optically active luminescence centres in ZnS nanoparticles. Therefore the luminescence intensity decreases when the Mn^{2+} concentration is 10%.

4.3. Fourier Transform Infra Red (FTIR) Spectroscopy:

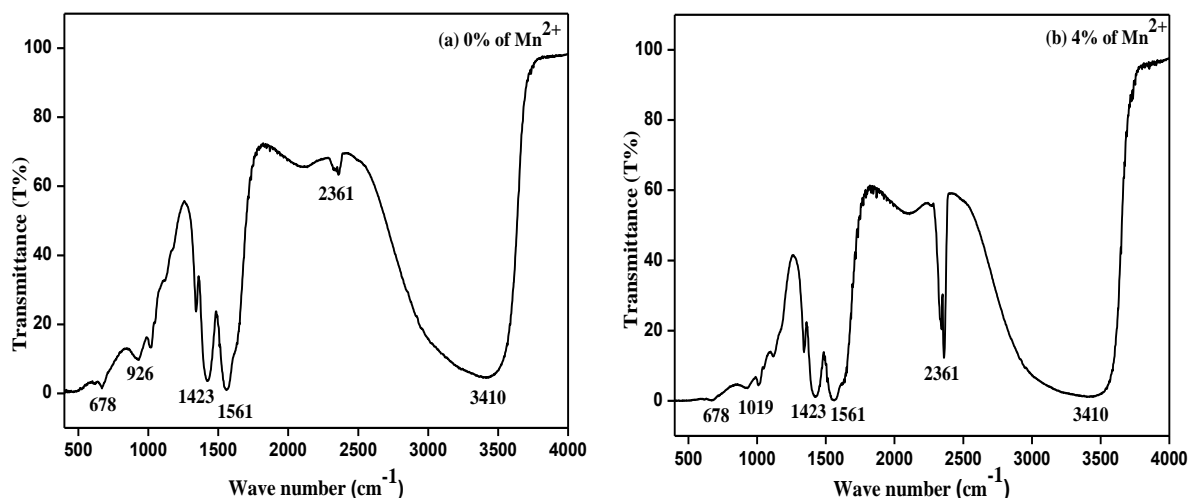


Figure 8 (a & b): FTIR spectra for undoped and 4% Mn²⁺ doped ZnS nanoparticles

Figure 8 (a & b) shows FTIR spectra for both undoped and Mn²⁺ doped ZnS nanoparticles in the range of 500 - 4000 cm⁻¹ which revealed the presence of capping agent. Analyzing the FTIR spectra of ZnS nanoparticles prepared for different dopant concentrations are almost similar and only negligible shifting is seen in the absorption peaks. Hence only one doped FTIR spectra is shown in figure 8(b) and from this one can observe many absorptions bands which are given in table 3.

Table 3: Vibrational mode of ZnS nanoparticles with positions and absorptions shown by IR spectra

Doping →	0%	4%	Mode of vibration
Position	3410	3410	O-H stretching band of the hydroxyl group
	2361	2361	O-H stretching band
	1561	1561	C-H stretching and bending bonds respectively which results to co-ordinate bonding between PVA and Zn indicating capping on ZnS
	1423	1423	
	926	1019	Oxygen stretching and bending frequency
	678	678	Zn-S stretching band

The absorption bands at 3410 cm⁻¹ in the spectra is due to OH⁻ stretching vibration band of water molecule absorb on the surface of the sample due to the presence of moisture. Bands at 2361cm⁻¹ is due to O-H stretching vibration. In additions the bands at 1561 cm⁻¹ and 1423 cm⁻¹ are due to C-H stretching and bending bonds respectively which results to co-ordinate bonding between PVA and Zn indicating capping on ZnS. There are also small narrow bands at 1019 cm⁻¹, 926 cm⁻¹ are due to the oxygen stretching and bending frequency and 678 cm⁻¹ indicates the presence of Zn-S stretching band. FTIR spectra of the synthesized samples yield the bands which are in good agreement with the reported values [38]. The FTIR spectra of 4% doped ZnS show that the absorption bands are almost similar with undoped ZnS except there is negligible shifting in the absorption peaks of all spectra due to interaction of ZnS molecules and Mn molecules.

V. Conclusion:

The synthesis of undoped and Mn²⁺ doped ZnS nanoparticles having sizes of 2.3 nm - 2.1 nm has been successfully synthesized by chemical co-precipitation method using PVA as capping agent. TEM images confirm the spherical shape with sizes of the range 3.45 nm – 5.47 nm. HRTEM images also clearly show the formation of lattice fringes indicating the crystalline nature of the synthesized sample. The SAED patterns confirm the cubic zinc blende structure which is in good agreement with the XRD pattern of ZnS. SEM images have shown a rough and spongy surface which is mainly due to passivation of PVA and hence makes it difficult to estimate the particle size. EDX analysis show the presence of Zinc and Sulphur for undoped ZnS nanoparticles and detectable amount of dopant in the Mn²⁺ doped ZnS nanoparticles. The optical energy band gaps calculated from the absorption spectra are found to be higher than that of bulk ZnS which show a blue shift with respect with the bulk value. This value shift can be attributed to quantum confinement effects in the crystals. The radii of the synthesized nanoparticles have been evaluated from the absorption spectrum by using EMA formula which corresponds well with the particle size calculated from XRD. The photoluminescence spectrum at room temperature showed a blue-green emission peaks at 430 nm and 501 nm whereas Mn²⁺ doped showed an orange emission peak at 618 nm under 340 nm excitation which is due to the Mn²⁺ ⁴T₁ - ⁶A₁

transition. The emission is found to increase with Mn²⁺ doping concentration upto 8% and then decreases. The presence of PVA molecules on the surface of ZnS: Mn nanoparticles are observed in FTIR spectra.

References:

- [1]. Weller, H; *Angew. Chem. Int. Ed. Engl.*, **1993**, 32,41
- [2]. Alvisatos, A.P., *Sciences*, **1996**, 271, 933
- [3]. Nirmal, M; Brus, L, *Acc. Chem. Res.*, **1999**, 32, 407
- [4]. Murray, C.B.; Norris, D.J.; Bewendi, M.G., *J. Am. Chem. Soc.*, **1993**, 115, 8706
- [5]. Peng, X, *Chem. Eur. J.*, **2002**, 8, 338
- [6]. Kumbhojkar, N; Nikesh, V.V.; Kashirasagar, A.; Mahamuni, S., *J. Appl. Phys.*, **2000**, 88, 6260
- [7]. Yamaguchi, T.; Yamamoto, Y., Tanaka, T.; Yoshida, A., *Thin Solid Films*, **1999**, 344, 516
- [8]. Liu, J.Z.; Yan, P.X.; Yue, G.H.; Chang, J.B.; Qu, D.M.; Zhuo, R.F., *J. Phys. D.*, **2006**, 39, 2352
- [9]. Lee, J.C.; Subramaniam, G; Lee, J.W.; Kang, T.W., *Appl. Phys. Lett.*, **2007**, 90, 262909
- [10]. Kulkarni, S.; Kazakova, O.; Holmes, J.D.; *Appl. Phys. A*, **2006**, 85, 277
- [11]. Hullavarad, N.V; Hullavarad, S.S; Karulkar, P.C, *J. Nanosci. Nanotechnol.*, **2008**, 6, 3272
- [12]. Chandramohon, S; Kamjilal, A; Tripathi, J.K.; Sarangi, S.N.; Sathyamoorthy, R.; Som, T., *Appl. Phys.*, **2009**, 4, 105
- [13]. Gaponeko, S.V., *Optical properties of semiconductor Nanocrystals*, Cambridge University Press, Cambridge, **1998**, 245
- [14]. Waggon, U, *Optical properties of semiconductor quantum dots*, Springer-Verlag, Berlin, **1996**, 250
- [15]. Ekimov, A.I; Efros, A.I; Onushchenko, A., A, *Solid State commun.*, **1985**, 56, 921
- [16]. Karan, N.; Suchitra, R.; Singh, F., *J. Cryst. Growth*, **2004**, 268, 585
- [17]. John, R.; Florence, S.S., *Chalcogenide Letters*, **2010**, 7(4), 269
- [18]. Ghosh, G.; Naskar, M.K.; Patra, A.; Chatterjee, M. *Optical Materials*, **2006**, 28, 1047
- [19]. Tamrakar, R.; Ramrakhiani, M; Chandra, B.P., *The Open Nanoscience Journal*, **2008**, 2, 12
- [20]. Yu I; Isobe T; Senna M, *Journal of Physics and Chemistry of Solids*, **1996**, 57(4), 373
- [21]. Klug, H.P.; Alexander, L.E., *X-ray Diffraction Procedures*, John Willey and Sons Inc. New York, **1954**, 3, 151.
- [22]. Cullity, B.D.; Stock, S.R., *Elements of X-ray diffraction*, Prentice Hall, New Jersey, 3rd edition, **2001**
- [23]. De, C.K., Mishra, N.K., *Indian J. Phys. A*, **1997**, 71, 530.
- [24]. Sen, S.; Halder, S.K.; Sen Gupta, S.P., *Jour. Phys. Soc. Japan*, **1975**, 38(6), 1643
- [25]. Rao, C.N.R.; Muller, A.; Cheetham, A.K. (Eds)., *The Chemistry of Nanomaterials*, Willey-VCH Verlag Gmbtt and Co. KgaA. Weinheim, **2005**, 2
- [26]. Nasr, T.B.; Kamoun, N.; Gusach, C., *Mater. Chem. Phys.*, **2006**, 96, 84.
- [27]. Chen, Jianfeng; Li, Yaling; Wang, Yuhong; Yum, Jimmy; Cao, Depeng, *Mater. Res. Bulletin*, **2004**, 39, 185.
- [28]. Thambidurai, M.; Muthukumarasamy, N; Agilan, S.; Murugan, N.; Vasantha, S.; Balasundaraprabhu, R.; Senthil, T.S., *J. Mater. Sci.*, **2010**, 45, 3254.
- [29]. Martinez- Castanon, G.A.; Sanchez- Lorendo, M.G.; Martinez-Mendoza, J.R.; Facundo Ruiz, *Advances in Tech. Mat. and Mat. Processing*, **2005**, 7(2), 171
- [30]. Yoffe, A.D., *Adv. Phys.*, **1993**, 42, 173
- [31]. Yuang, Y.S.; Chen, F.Y.; Lee, Y.Y.; Liu, C.L., *Jpn. J. Appl. Phys.*, **1994**, 76, 304.
- [32]. Gan, L.M.; Liu, B.; Chew, C.H.; Xu, S.J.; Chua, S.J.; Xu, G.Q., *Applied Physics Letters*, **1998**, 73(4), 478
- [33]. Cao, J.; Yang, J.; Zhang, Y; Wang, Y.; Wet, M.; Liue, Y.; Gao, M.; Liu, X.; Xie, Z., *J. Alloy Compd.*, **2009**, 486, 890
- [34]. Xiao, Q.; Xiao, C., *Appl. Surf. Sci.*, **2008**, 254, 6432
- [35]. Peng, WQ; Qu, SC; Cong, GW; Zhang, XQ; Wang, ZG, *J. Cryst. Growth*, **2005**, 279, 454
- [36]. Murgados, G.; Rajamannan, B.; Ramasamy, V., *J. Lumin.*, **2010**, 130, 2032
- [37]. Elham, Mohaghehpour; Mohammad, Rabiee; Fathollah ,Mohtarzadeh; Mohammardreza, Tahriiri, *Journal of Ceramic Processing Research*, **2010**, 11(2), 144
- [38]. Mote, V.D.; Purushotham Y.; Dole B.N., *Ceramica*, **2013**, 59, 395